IN-39

/. / 3

P.15

Numerical Calibration of the Stable Poisson Loaded Specimen

Louis J. Ghosn
Sverdrup Technology, Inc.
Lewis Research Center Group
Brook Park, Ohio

Anthony M. Calomino
National Aeronautics and Space Administration
Lewis Research Center
Cleveland, Ohio

and

Dave N. Brewer
Propulsion Directorate
U.S. Army Aviation Systems Command
Lewis Research Center
Cleveland, Ohio

N93-12733

(NASA-TM-105609) NUMERICAL
CALIBRATION OF THE STABLE POISSON
LOADED SPECIMEN (NASA) 15 p

October 1992

Unclas

G3/39 0129293

NASA

NUMERICAL CALIBRATION OF THE STABLE POISSON LOADED SPECIMEN

Louis J. Ghosn
Sverdrup Technology, Inc.
Lewis Research Center Group
Brook Park, Ohio 44142

Anthony M. Calomino
National Aeronautics and Space Administration
Lewis Research Center
Cleveland, Ohio 44135

and

Dave N. Brewer
Propulsion Directorate
U.S. Army Aviation Systems Command
Lewis Research Center
Cleveland, Ohio 44135

E-7335

ABSTRACT

An analytical calibration of the Stable Poisson Loaded (SPL) specimen is presented. The specimen configuration is similar to the ASTM E-561 compact-tension specimen with displacement controlled wedge loading used for R-Curve determination. The crack mouth opening displacements (CMOD's) are produced by the diametral expansion of an axially compressed cylindrical pin located in the wake of a machined notch. Due to the unusual loading configuration, a three-dimensional finite element analysis was performed with gap elements simulating the contact between the pin and specimen. In this report, stress intensity factors, CMOD's, and crack displacement profiles, are reported for different crack lengths and different contacting conditions. It was concluded that the computed stress intensity factor decreases sharply with increasing crack length thus making the SPL specimen configuration attractive for fracture testing of brittle, high modulus materials.

INTRODUCTION

The ability to promote stable crack growth in brittle materials is hindered by the flexibly of the loading fixture and high stiffness to fracture toughness ratio of the test specimen. By increasing the crack front width with increasing crack length, the Chevron-Notched crack geometries (fig. 1(a)) offer a solution to initiating and growing a stable crack in ceramic materials (ref. 1). Unfortunately, the variation in the crack width with increasing crack length makes an R-curve type of analysis tedious (ref. 1). An alternative technique for establishing stable growth is displacement controlled wedge loading (ref. 2). Stability is accomplished by imposing a theoretically constant displacement at the crack mouth causing a decrease in stress intensity factors with increasing crack length. The conventional wedge loading configuration (fig. 1(b)) for a double beam was experimentally attempted and found to be ineffective in producing a stable crack in brittle materials with high elastic moduli because the loading train is in series with the specimen. The strain energy stored in the loading fixture, which is released during fracture, is often enough to cause a catastrophic failure. A solution for minimizing the effect of stored energy is to taper the specimen height (fig. 1(c)). The tapered section amplifies the trend of decreasing stress intensity factors with increasing crack length (ref. 3). However, the tapered angle chosen must be a function of the loading train stiffness (specimen included) and the specimen fracture toughness. In addition to this

geometric tailoring, side grooves are often used to artificially produce rectilinear crack growth. The exact effect of side grooving on measured fracture strength properties is still unknown and debatable (ref. 4).

A recently introduced displacement controlled wedge loading alternative which produces stable crack growth in brittle materials is the Stable Poisson Loaded (SPL) configuration developed by Calomino and Brewer (ref. 5). The load train stiffness is isolated from the specimen by loading a cylindrical pin that is fitted in the wake of the notched specimen (fig. 2). The specimen is wedge loaded by the diametral Poisson expansion of the compressed cylindrical pin. This novel loading configuration has been applied successfully to promote stable crack growth in ceramic materials such as aluminum oxide and silicon nitride (ref. 6). The specimen geometry is similar to the compact tension geometry and does not require side grooving to produce rectilinear crack growth. The loading concept is similar to the ASTM E-561 compact tension under controlled wedge loading (ref. 7).

The purpose of this work is to present the numerical calibration of the SPL specimen using the finite element method. Two specimen configurations were analyzed: the original SPL with a small machined notched width ($N \approx 0$), and the modified SPL with a larger notched width ($N = 1.77$ mm). The SPL specimen configuration with $N \approx 0$ results in a contacting area equal to $2\pi Rb$, where R is the radius of the pin and b is the specimen thickness. Experimental results (ref. 6) indicated that the larger pin-to-specimen contact area in the original SPL specimen introduced frictional forces which affected the fracture toughness measurements with increasing crack length. To minimize the frictional effect at the pin-to-specimen interface, the machined notch width was enlarged in the modified geometry ($N = 1.77$ mm), which reduced the contacting area to $\pi Rb/2$. Both specimens were analyzed to provide an insight in the stability of the SPL geometries.

NUMERICAL PROCEDURE

Three-dimensional finite element meshes were generated to analyze the two SPL specimen geometries. The ceramic specimen and the steel loading pin dimensions used are shown in figure 2. Two types of notched geometries were analyzed. In the original configuration, the machined notch width was 0.5 mm which was taken to be zero for modeling purposes. In the modified SPL geometry the machined notch was enlarged ($N = 1.77$ mm) to minimize frictional effects. The geometrical symmetry permitted one quarter of the specimens to be modeled yielding 280 isoparametric 20-noded elements, 1966 nodes for the original SPL specimen, and 302 elements with 2196 nodes for the modified geometry. Typical meshes for both the modified and original SPL specimens are shown in figures 3(a) and 3(b), respectively. Only one element through the specimen thickness was used since the parabolic displacement allowed with this type of element usually gives good solutions for both stresses and displacements (ref. 8). The mesh density near the crack tip is relatively high in order to accurately capture the stress singularity. At the crack tip, quarter-point elements were employed. The central nodes on the edges adjacent to the crack front were moved to one-quarter the length of the edge as measured from the crack tip to capture the square-root singularity (ref. 9). The ratio of the length of the singularity element over the crack length was always kept equal to 0.0097 for all the crack lengths considered.

The stress analysis was conducted with five different sets of constraints imposed along the interface of the two materials due to the uncertainty of the contact condition between the steel pin and the specimen. Nodes along the contacting interface were duplicated to facilitate implementation of the different boundary conditions. One set of these nodes was associated with specimen elements, and another set was associated with pin elements.

2

The contact between the pin and the specimen was modeled with five different specimen-to-pin interface boundary conditions: free, fully tied, radial tying, gap element without friction, and gap element with friction. Only one coulomb frictional coefficient of $\mu = 0.40$ was considered in this analysis. The simplest specimen-to-pin boundary condition (free) linked only the central node along the contacting area of the two bodies considered. A fully-tied boundary condition assumed that all contacting nodal degrees of freedom for one body were attached to the opposing nodes for the second body. A radial tying boundary condition, on the other hand, assumed that only the radial degree of freedom for each pair of nodes are coupled after transformation to a local cylindrical coordinate system. Another contacting option considered in this study was the use of a special gap-link element provided by the general purpose finite element program MARC (ref. 8). This element allows separation or contact to occur between the two bodies depending on the forces along the link. If the force is tensile, the link provides for separation of the two bodies resulting in no transmitted forces. If the force is compressive, the gap closes, and a radial force is transmitted. If the friction option is chosen with the gap elements, coulomb type frictional forces are generated as the gap closes. The magnitude of the frictional shear force is linearly proportional to the normal force, with μ being the coulomb friction coefficient. Thus, material contact produces a frictional shear force tangent to the interface between the two bodies. The original SPL specimen required a total of 24 gap elements, while the modified geometry used only eight gap elements. The gap elements were implemented only on the contacting corner nodes of each 20-node brick element, along the specimen-to-pin interface. The mid-nodes purposely were not linked to prevent oscillation of displacements and force a linear displacement variation along the element.

The stress intensity factor (SIF) was determined as a function of crack length from the crack tip opening displacement as well as the J-integral approach. The SIF for the free contacting option was also calculated using the compliance method for comparison. The plane strain SIF from the crack-tip opening displacement is given by the following equation (ref. 9):

$$K_I = \frac{E_c}{4\left(1 - \nu_c^2\right)} \sqrt{\frac{2\pi}{\ell}} \left[4 \, V_b - V_c\right] \tag{1}$$

where ℓ is the length of the singularity element and V_b and V_c are the half opening displacements at the 1/4 and corner nodes of the singularity element along the crack front, respectively. The variables E_c and ν_c denote the specimen Young's modulus and Poisson's ratio, respectively.

The J-integral is calculated from the change in strain energy due to a small perturbation of the nodes around the crack tip (ref. 10). A total of 616 nodes are displaced near the crack tip to determine the SIF using the following equation:

$$K_I = \sqrt{G_I \frac{E_c}{\left(1 - \nu_c^2\right)}} = \sqrt{\left[\frac{1}{b} \frac{\Delta U}{\Delta a}\right] \frac{E_c}{\left(1 - \nu_c^2\right)}} \tag{2}$$

where ΔU is the change in strain energy, Δa is the change in crack length, b is the specimen thickness, and G_I is the mode I energy release rate.

3

RESULTS

The finite element analysis was conducted for both the steel loading pin and the high elastic modulus specimen. The elastic properties for both materials are shown in table I. A uniform axial compressive pressure was applied to the pin produced a diametral expansion effectively wedging open the crack. The SIF and the crack opening displacements (COD) are determined for different normalized crack lengths, a/W, ranging from 0.25 to 0.90. The analysis was conducted for both the original SPL specimen with a machined notch width nearly equal to zero and the modified specimen with the larger notch (N = 1.77 mm).

Load Transfer

The load transferred to the specimen from the pin's radial expansion was calculated by summing nodal reaction forces in the Y-direction (fig. 3(a)) along the symmetry plane of the pin (the Y = 0 plane of the pin). The ratio of the load transferred to the specimen, P_{sp}, to the applied pin load, P_a, is shown in figure 4 as a function of a/W for each contact boundary condition. The data displayed in figure 4 was limited to the modified SPL specimen, as this represents the preferred test geometry. All contact conditions between the loading pin and the specimen revealed decreasing transferred loads with increasing crack length for a given applied compressive pin loading, demonstrating the fracture stability of the specimen. The decreasing trend in transferred load was consistent with increasing specimen compliance. The fully-tied contact option always supplied the largest transferred load.

Crack Opening Profiles

COD profiles were evaluated for each contact condition in the analysis of the modified SPL specimen. These results are shown in figures 5(a) to 5(e) as a function of the distance measured from the pin's center. The half crack opening displacement V was normalized with respect to E_c (the modulus of the ceramic specimen), b, and P_{sp}. Local deformations in the area of the pin were evaluated for each contact option considered.

The large deformations in the pin region, evaluated for the fully-tied case, represent a stretching of the material. These deformations were the result of the imposed contact conditions at the interface. Such deformations are unrealistic since large tensile forces are exerted to keep the specimen in contact with the pin. Deformations near the pin for the radial-tying case (fig. 5(b)) also suggests the presence of tensile forces across the pin-to-specimen interface, although the magnitudes are considerably lower than that for the fully-tied case. Similar displacement profiles are observed for the same contact conditions in the original specimen, although not shown.

The smoothest crack opening profile displayed (fig. 5(c)) was produced by the free contact case, where only the central node of the pin is attached to the specimen. Very similar crack opening profiles were seen for the gap element solutions (fig. 5(d)) without friction and (fig. 5(e)) with friction. These three contact conditions result in small changes in local deformations near the pin and do not alter the overall crack opening displacement profiles. All three crack opening profiles compare well with each other.

Normalized half opening displacements at two specific locations along the crack front are plotted in figures 6(a) and 6(b). The displacement, designated V_1 in figure 6(a), refers to the displacement at the free edge of the specimen located behind the pin at a distance x = −10 mm. This displacement is also referred to as the crack mouth opening displacement (CMOD). The displacement denoted V_2 in figure 6(b)

4

is the crack opening evaluated at a distance $x = 7.0$ mm ($a/W = 0.2$) in front of the pin. The fully-tied case results in smaller opening displacements than the other contacting options, which is an effect of the tensile forces across the contacting bodies. Both displacements, V_1 and V_2, increase with increasing crack length for all considered contact conditions. The normalized opening displacements of the radial-tying and the free case were almost identical for both locations. The opening displacements for the gap elements with- and without-friction were slightly lower. They are, however, still higher than the fully tied case. Since the load transferred to the specimen is difficult to measure experimentally, the ratio of V_1 over V_2 as plotted in figure 7 can be used to obtain the crack length through nonvisual techniques as suggested by ASTM E-561 standard (ref. 7).

Stress Intensity Factor

The stress intensity factors for the modified specimen with the free contact condition case are given in table II as a function of crack length. Listed in table II are the results of three techniques used to calculate SIF values: the J-integral method, the crack opening displacement in the singular element immediately adjacent to the crack tip, and finally the compliance method. The SIF from the compliance method was determined from the change in the work done by the external force with increasing crack length. For the free case, the normalized compliance was taken at the only node of the specimen attached to the pin. The normalized SIF factor from the compliance method is then given by:

$$Y = \frac{K_I \, b \, \sqrt{w}}{P_{sp}} = \sqrt{\frac{1}{2} \frac{d \dfrac{2 E_c V_b}{P_{sp}}}{d \dfrac{a}{W}}}$$ (3)

where V is half the opening displacement at the center of the contacting bodies, and the derivative of the compliance is determined here numerically using the central difference formula (ref. 11).

As seen in table II, the variation in the normalized SIF between the J-integral and the displacement methods is less than 4 percent for a normalized crack length ranging from 0.4 to 0.9. The difference increases to 9.7 percent for the shorter crack length. The difference in the SIF, comparing now the J-integral approach to the compliance method, is less than 4 percent for a/W ratios between 0.30 to 0.80. The difference increases to 9.6 percent at the larger crack length, $a/W = 0.85$. The compliance method is affected by the sharp increase in displacement near the free edge.

In summary, the variation between the numerically determined SIF values from the three different methods is within 6 percent for a/W ranging from 0.3 to 0.8, demonstrating a confidence in the results within this range. Discrepancies at short and long crack lengths were attributed to the free edge effects and the sharp gradient in the opening displacement for the deep cracks.

Having shown similarity in the results using the three different methods for the free contact option, the values of the SIF for all other contact options were calculated for the modified SPL specimen and are presented in figure 8. Since the J-integral method has proven to be highly accurate even with a coarse mesh (ref. 10), it is the preferred method for computing the SIF results. The reported SIF values were normalized with respect to the load transferred to the specimen P_{sp} and evaluated using only the J-integral approach.

The SIF values for the fully-tied case were always lower than the other contact options. This trend was expected since this fully tied case exerted tensile forces between the pin and the specimen. Also shown in the figure 8 are the SIF results for the Compact Tension (CT) specimen from reference 12. The comparison is adequate since the geometry of the SPL specimen is very similar to the CT specimen. The excellent agreement between the present analysis and the CT specimen increases the confidence in the numerical procedure adopted here.

Since the load transferred to the specimen from the pin is experimentally difficult, if not impossible, to measure, the SIFs were normalized with respect to the E_c and the free edge half opening displacement V_1, $(K_I\sqrt{W}/E_c V_1)$. These are re-plotted in figures 9(a) and 9(b) for the modified and the original specimens, respectively. As seen from the figures, there is a sharp drop in the stress intensity factor with increasing crack length under a constant applied displacement condition. The reduction in stress intensity factor was about 75 percent, making the SPL specimen geometry very attractive for fracture toughness testing of brittle materials. The variation in the SIF for the modified specimen was much smaller than the original specimen for a given a/W ratio, for the three contacting options shown. When the notched width was small ($N \approx 0$), the pin introduces additional constraints on the free opening of the specimen. This additional constraint is responsible for much wider SIF variations at smaller crack lengths. The variation in the SIF for the original specimen between the free and radial tying were isolated as the source of large experimental scatter in the fracture toughness measurements (ref. 6). The modified specimen provided more consistent SIF results, irrespective of the contacting options used as seen in figure 9(a).

The numerical results needed for experimental calibration of the modified SPL specimen are given in table III assuming the frictional gap contacting condition with $\mu = 0.4$. Although the actual frictional forces at the pin-to-specimen interface are not known, its effect is felt to be well modeled since the solutions are bounded within a narrow region. The gap element option with friction is considered the most realistic simulation of actual experimental contacting conditions. Shown in table IV are the best fit equations of the results presented in table III for experimental applications.

CONCLUSIONS

A three-dimensional stress analysis was conducted on the original and the modified SPL specimens. The stress intensity factor calculation for the modified specimen configuration, with a reduced pin-to-specimen contact area, showed relatively small dependence on the interaction between the loading pin and the specimen. The SIF of the original specimen design, which incorporated a larger contact area between the loading pin and the specimen, showed a larger sensitivity to the type of contact assumed.

By increasing the contact area, the pin introduces additional constraints on the free opening of the specimen. This observation is consistent with the large scatter observed in the previously reported fracture toughness measurements, which utilized the original SPL specimen design.

The modified SPL specimen configuration is very stable and attractive for fracture testing of brittle materials since the SIF is reduced by more than 75 percent for a crack extension from a normalized crack length, a/W of 0.25 to 0.90, under constant displacement conditions.

REFERENCES

1. Newman, J.C., Jr.: A Review of Chevron-Notched Fracture Specimens. Chevron-Notched Specimens Testing and Stress Analysis, ASTM STP–855, J.H. Underwood, S.W. Freiman, and F.I Baratta, eds., American Society for Testing and Materials, Philadelphia, PA, 1984, pp. 5–31.

2. Hahn, G.T., et al.: A Preliminary Study of Fast Fracture and Arrest in DCB Test Specimen. Dynamic Crack Propagation, G.S. Sih, ed., Noordhoff, Leyden, 1973, pp. 649–662.

3. Crosley, P.B.; and Ripling, E.J.: Significance of Crack Arrest Toughness (K_{Ia}) Testing. Crack Arrest Methodology and Applications ASTM STP–711, G.T. Hahn and M.F. Kanninen, eds., American Society for Testing and Materials, Philadelphia, PA, 1980, pp. 321–337.

4. Annis C.G.; and Cargill, J.S.: Modified Double Torsion Method for Measuring Crack Velocity in NC–132 (Si_3N_4). Fracture Mechanics of Ceramics, Vol. 4, R.C. Bradt, D.P.H. Hasselman, and F.F. Lange, eds., Plenum Press, New York, 1974, pp. 737–744.

5. Calomino, A.M.; and Brewer, D.N.: Controlled Crack Growth Specimen for Brittle Systems. J. Am. Ceram. Soc., vol. 75, no. 1, 1992, pp. 206–208.

6. Calomino, A.M.; Brewer, D.N.; and Ghosn, L.G.: Fracture Behavior of Ceramics Under Displacement Controlled Loading. NASA TM–105565, 1992.

7. Standard Practice for R-Curve Determination. ASTM E 561–86, 1990 Annual Book of ASTM Standards, Metals Test Methods and Analytical Procedures, vol. 03.01, ASTM, Philadelphia, PA, pp. 571–582.

8. MARC General Purpose Finite Element Program, Version K.4, MARC Analysis Research Corporation, Palo Alto, CA, Jan. 1990.

9. Barsoum, R.S.: On the Use of Isoparametric Finite Elements in Linear Fracture Mechanics. Int. J. Numer. Methods Eng., vol. 10, 1976, pp. 25–38.

10. Parks, D.M.: A Stiffness Derivative Finite Element Technique for Determination of Elastic Crack Tip Stress Intensity Factors. Int. J. Fract., vol. 10, no. 4, Dec. 1974, pp. 487–502.

11. Conte, S.D.; and De-Boor, C.: Elementary Numerical Analysis (An Algorithmic Approach). Third ed., McGraw-Hill Book Co., New York, 1980.

12. Srawley, J.E.: Wide Range Stress Intensity Factor Expressions for ASTM E 399 Standard Toughness Specimens. Int. J. Fract. Mech., vol. 12, June 1976, pp. R475–R476.

TABLE I.—ELASTIC MATERIAL PROPERTIES
ASSUMED

	Modulus, E GPa	Poisson ratio, ν
Brittle specimen	350	0.25
Loading pin	207	0.30

TABLE II.—NORMALIZED SIF FOR THE MODIFIED SPL SPECIMEN

ASSUMING A FREE CONTACTING OPTION

Normalized crack length	Normalized stress intensity factor, $\dfrac{K_I b \sqrt{W}}{P_{sp}}$				
a/W	J-Integral	Displacement		Compliance	
0.25	5.351	4.833	-9.7%[*]	-------	-------
0.30	5.905	5.565	-5.7%	5.749	-2.6%[*]
0.35	6.579	6.202	-5.7%	6.411	-2.6%
0.40	7.412	7.181	-3.7%	7.233	-2.4%
0.45	8.460	8.327	-1.6%	8.269	-2.3%
0.50	9.807	9.744	-0.6%	9.605	-2.1%
0.55	11.577	11.565	-0.1%	11.372	-1.8%
0.60	13.973	13.998	0.2%	13.777	-1.4%
0.65	17.320	17.367	0.3%	17.350	-0.2%
0.70	22.201	22.238	0.2%	22.190	-0.1%
0.75	29.737	29.693	-0.1%	30.017	0.9%
0.80	42.370	42.036	-0.8%	43.977	3.8%
0.85	66.461	65.141	-2.0%	72.825	9.6%
0.90	123.978	119.415	-3.7%	-------	-------

[*]Indicates percent difference from the J-integral values.

$\dfrac{a}{W}$	$\dfrac{V_1}{V_2}$	$\dfrac{P_{sp}}{P_a}$	$\dfrac{E_c\,V_1\,b}{P_{sp}}$	$\dfrac{E_c\,V_2\,b}{P_{sp}}$	$\dfrac{K_I\,b\,\sqrt{W}}{P_{sp}}$	$\dfrac{K_I\,\sqrt{w}}{E_c\,V_1}$
0.25	4.082	1.17E-2	7.98	1.96	5.334	0.6684
0.30	3.128	1.43E-2	10.12	3.23	5.881	0.5814
0.35	2.727	1.19E-2	11.49	4.21	5.916	0.5148
0.40	2.491	9.85E-2	15.93	6.40	7.359	0.4619
0.45	2.329	8.06E-3	20.03	8.60	8.382	0.4185
0.50	2.206	6.51E-3	25.38	11.51	9.690	0.3817
0.55	2.108	5.15E-3	32.62	15.48	11.403	0.3495
0.60	2.026	3.98E-3	42.81	21.13	13.702	0.3201
0.65	1.956	2.97E-3	57.82	29.56	16.883	0.2920
0.70	1.896	2.13E-3	81.23	42.84	21.444	0.2640
0.75	1.844	1.44E-3	120.35	65.27	28.299	0.2351
0.80	1.798	9.07E-3	191.84	106.67	39.251	0.2046
0.85	1.759	5.13E-3	338.92	192.71	58.208	0.1717
0.90	1.724	2.50E-3	693.26	402.14	93.892	0.1354

9

$$\frac{V_1}{V_2} = \frac{2.9225 - 16.0472\left(\frac{a}{W}\right) - 18.8965\left(\frac{a}{W}\right)^2}{1 - 1.5373\left(\frac{a}{W}\right) - 18.7505\left(\frac{a}{W}\right)^2}$$

$$\frac{P_{sp}}{P_s} = \begin{array}{c} 0.01722 - 0.04368\left(\frac{a}{W}\right) + 0.02391\left(\frac{a}{W}\right)^2 \\[2mm] + \dfrac{0.002821}{\left(\frac{a}{W}\right)} - \dfrac{0.0001230}{\left(\frac{a}{W}\right)^2} \end{array}$$

$$\frac{E_c V_1 b}{P_{sp}} = \frac{1.7782 + 12.0723\left(\frac{a}{W}\right) - 7.0620\left(\frac{a}{W}\right)^2}{1. - 2.0439\left(\frac{a}{W}\right) + 1.0488\left(\frac{a}{W}\right)^2}$$

$$\frac{E_c V_2 b}{P_{sp}} = \frac{- 1.3638 + 11.4968\left(\frac{a}{W}\right) - 6.7593\left(\frac{a}{W}\right)^2}{1. - 2.0674\left(\frac{a}{W}\right) + 1.0733\left(\frac{a}{W}\right)^2}$$

$$\frac{K_I b\sqrt{W}}{P_{sp}} = - 3.1674 - 9.2761\sqrt{\left(\frac{a}{W}\right)}\, \ell n\left(\frac{a}{W}\right) - 11.2990\frac{\left(\frac{a}{W}\right)}{\ell n\left(\frac{a}{W}\right)}$$

$$\frac{K_I \sqrt{W}}{E_c V_1} = \begin{array}{c} 1.5012 - 5.2140\left(\frac{a}{W}\right) + 9.4063\left(\frac{a}{W}\right)^2 \\[2mm] - 8.2054\left(\frac{a}{W}\right)^3 + 2.5760\left(\frac{a}{W}\right)^4 \end{array}$$

10
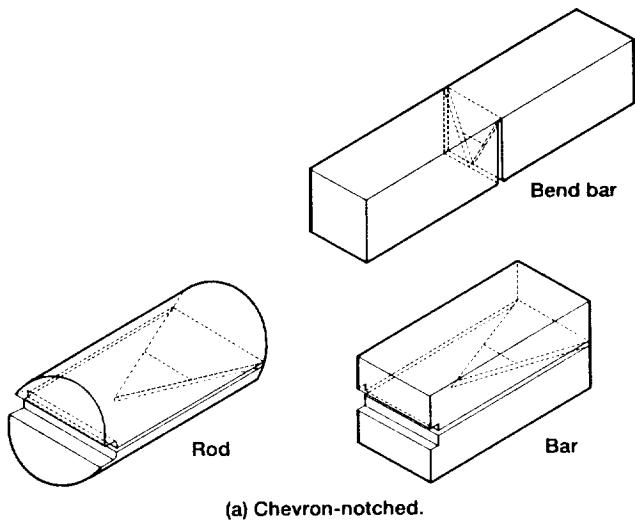
(a) Chevron-notched.
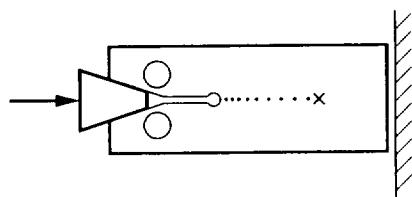
(b) Wedged double cantilever beam.
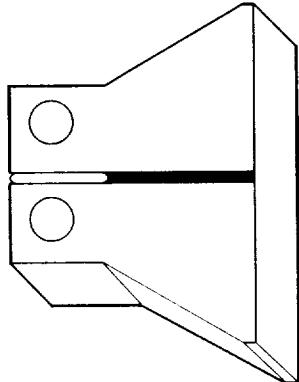
(c) Tapered cantilever beam.

Figure 1.—Various fracture specimen configurations for brittle materials.

2H = 45 mm
W = 35 mm
b = 2 mm
2R = 5 mm
w' = 10 mm
N = 0, 1.77 mm
s = 4 mm
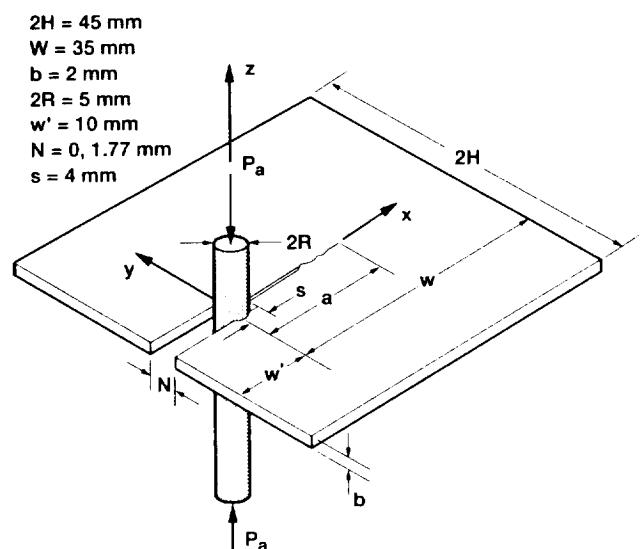
Figure 2.—Modified stable poisson loading specimen configuration.
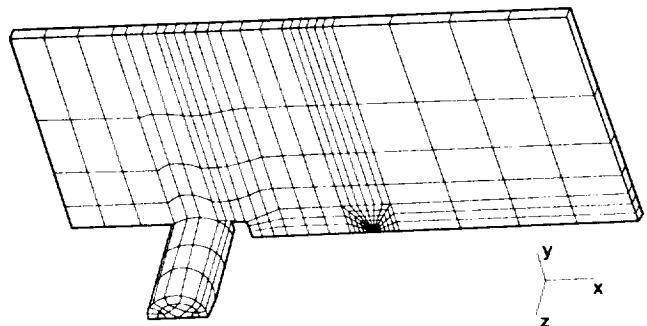
(a) Modified specimen, a/W = 0.4.
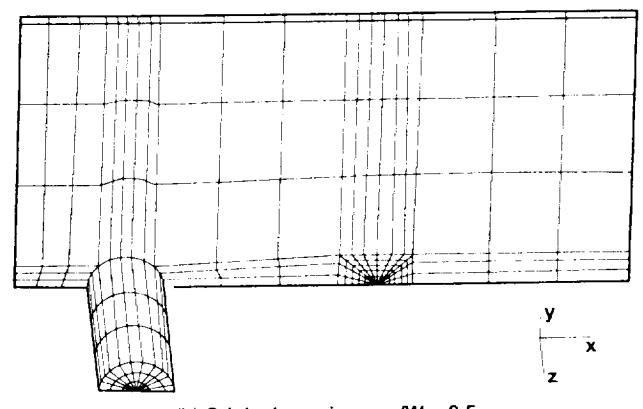
(b) Original specimen, a/W = 0.5.

Figure 3.—Finite element mesh for the stable poisson loading specimen.
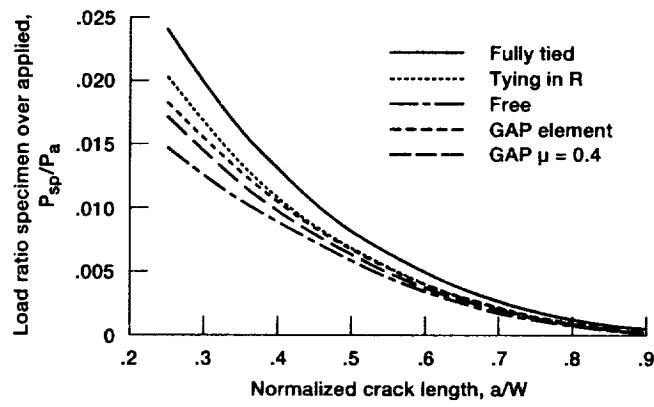
Figure 4.—Ratio of the load transferred to the specimen over the applied load to the pin (P_{sp}/P_a) for different contacting options for the modified SPL specimen.

(a) Fully tied case.

(b) Radial tying.

(d) Gap elements.

(c) Free.

(e) Gap elements with friction, $\mu = 0.4$.
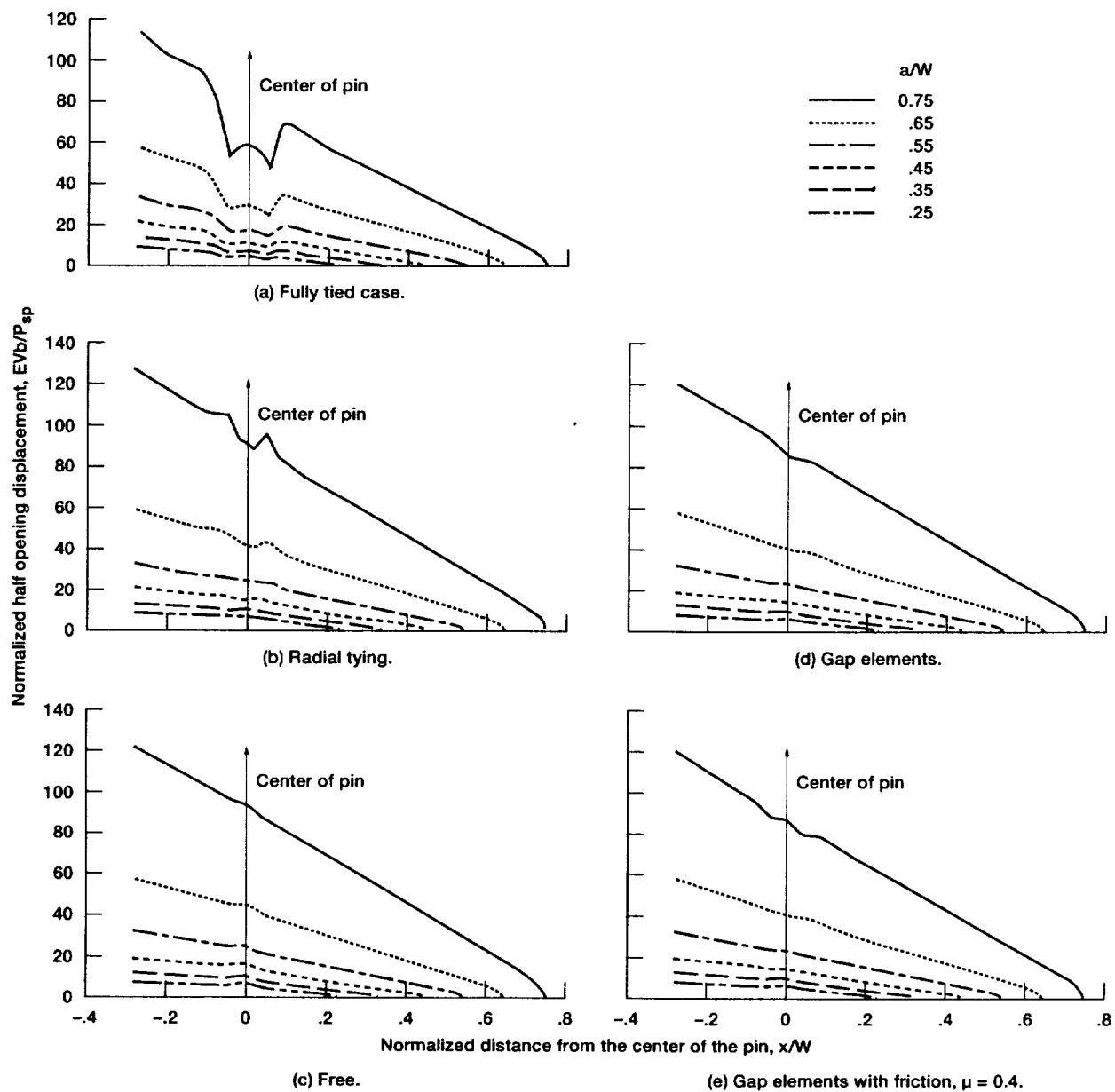
Figure 5.—Normalized half crack opening profiles as a function of the normalized distance from the center of the pin for different crack lengths for the modified SPL specimen.

12

(a) V_1 measured at x = -10 mm.

(b) V_2 measured at x = 7 mm.
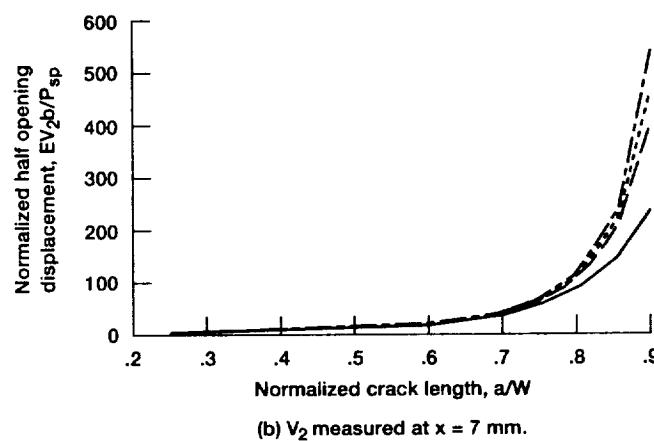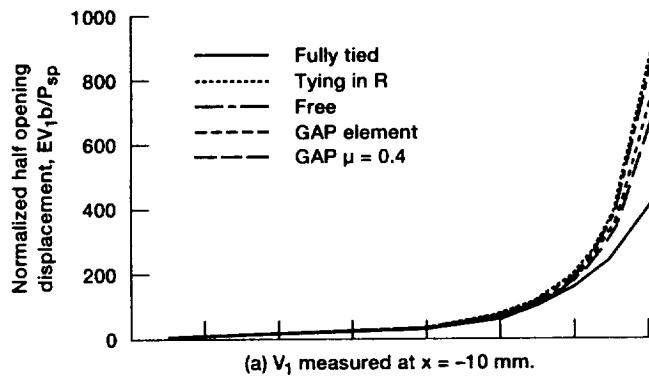
Figure 6.—Normalized half opening displacements as a function of crack lengths for different contacting options for the modified SPL specimen.
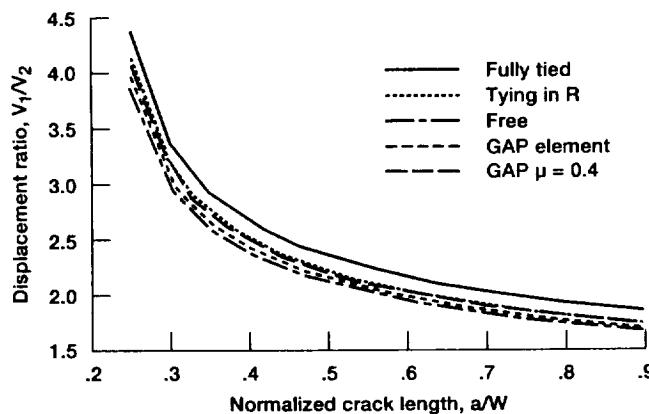
Figure 7.—Ratio of the opening displacement V_1 over V_2 at two different locations as a function of the normalized crack length for the modified specimen.
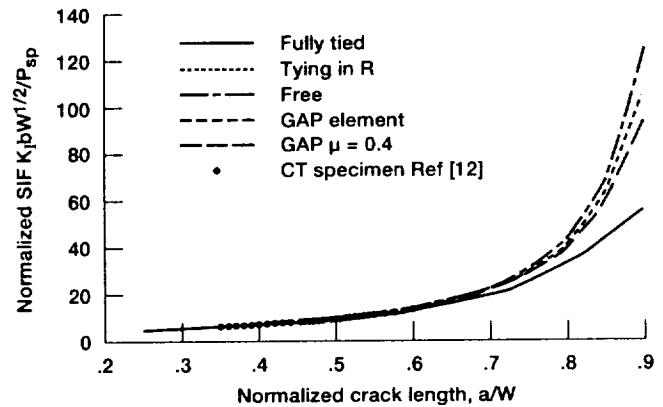
Figure 8.—Normalized stress intensity factor with respect to the load transferred to the specimen as a function of crack lengths for different contacting options for the modified SPL specimen.

(a) Modified SPL specimen.

(b) Original SPL specimen.
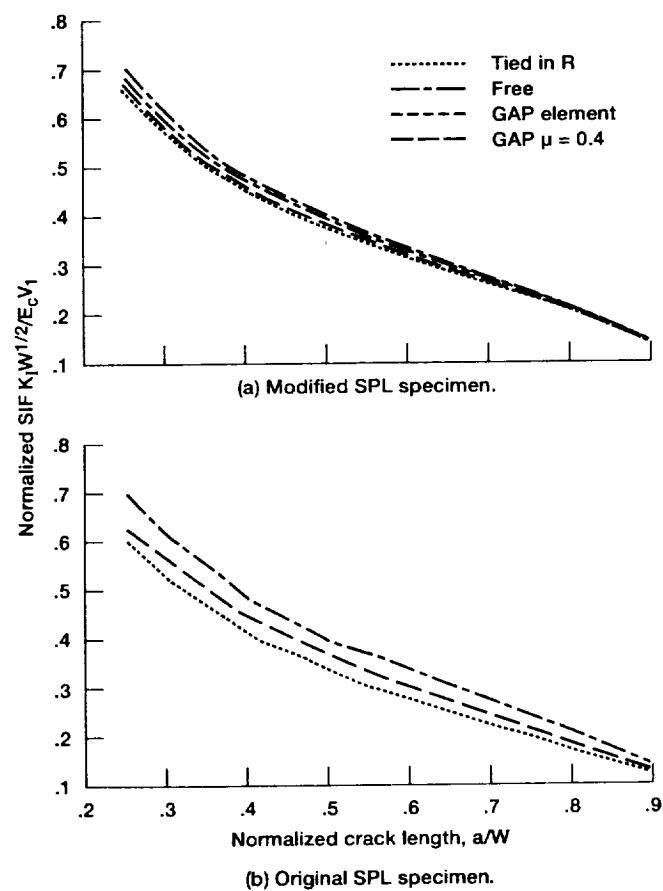
Figure 9.—Normalized stress intensity factor with respect to the free edge opening displacement as a function of crack lengths for different contacting options.

13

REPORT DOCUMENTATION PAGE

Form Approved
OMB No. 0704-0188

1. AGENCY USE ONLY (Leave blank)	2. REPORT DATE October 1992	3. REPORT TYPE AND DATES COVERED Technical Memorandum

4. TITLE AND SUBTITLE

Numerical Calibration of the Stable Poisson Loaded Specimen

5. FUNDING NUMBERS

WU–505–63–5B

6. AUTHOR(S)

Louis J. Ghosn, Anthony M. Calomino, and Dave N. Brewer

7. PERFORMING ORGANIZATION NAME(S) AND ADDRESS(ES)

National Aeronautics and Space Administration
Lewis Research Center
Cleveland, Ohio 44135–3191

8. PERFORMING ORGANIZATION REPORT NUMBER

E–7335

9. SPONSORING/MONITORING AGENCY NAMES(S) AND ADDRESS(ES)

National Aeronautics and Space Administration
Washington, D.C. 20546–0001

10. SPONSORING/MONITORING AGENCY REPORT NUMBER

NASA TM–105609

12a. DISTRIBUTION/AVAILABILITY STATEMENT

Unclassified - Unlimited
Subject Category 39

12b. DISTRIBUTION CODE

13. ABSTRACT (Maximum 200 words)

An analytical calibration of the Stable Poisson Loaded (SPL) specimen is presented. The specimen configuration is similar to the ASTM E–561 compact-tension specimen with displacement controlled wedge loading used for R-Curve determination. The crack mouth opening displacements (CMOD's) are produced by the diametral expansion of an axially compressed cylindrical pin located in the wake of a machined notch. Due to the unusual loading configuration, a three-dimensional finite element analysis was performed with gap elements simulating the contact between the pin and specimen. In this report, stress intensity factors, CMOD's, and crack displacement profiles, are reported for different crack lengths and different contacting conditions. It was concluded that the computed stress intensity factor decreases sharply with increasing crack length thus making the SPL specimen configuration attractive for fracture testing of brittle, high modulus materials.

14. SUBJECT TERMS	15. NUMBER OF PAGES
Finite-element; Stress intensity factor; Brittle materials; Fracture toughness testing; Stable specimen	14
	16. PRICE CODE A03

17. SECURITY CLASSIFICATION OF REPORT Unclassified	18. SECURITY CLASSIFICATION OF THIS PAGE Unclassified	19. SECURITY CLASSIFICATION OF ABSTRACT Unclassified	20. LIMITATION OF ABSTRACT